

Article

A Novel Sensorless Control Strategy for Brushless Direct Current Motor Based on the Estimation of Line Back Electro-Motive Force

Chengde Tong ^{1,2} , Mingqiao Wang ¹ , Baige Zhao ³, Zuosheng Yin ¹ and Ping Zheng ^{1,4,*}

¹ School of Electrical Engineering and Automation, Harbin Institute of Technology, Harbin 150080, China; tongchengde@hit.edu.cn (C.T.); 18846186348@163.com (M.W.); yinzuosheng0102@163.com (Z.Y.)

² School of Astronautics, Harbin Institute of Technology, Harbin 150080, China

³ 704 Institute, China Shipbuilding Industry Corporation, Xuhui District, Shanghai 200030, China; zbg hit@163.com

⁴ State Key Laboratory of Robotics and System, Harbin Institute of Technology, Harbin 150080, China

* Correspondence: zhengping@hit.edu.cn; Tel.: +86-451-8640-3086

Received: 4 August 2017; Accepted: 8 September 2017; Published: 12 September 2017

Abstract: In this paper, a novel sensorless control strategy based on the estimation of line back electro-motive force (BEMF) is proposed. According to the phase relationship between the ideal commutation points of the brushless direct current motor (BLDCM) and the zero-crossing points (ZCPs) of the line BEMF, the calculation formula of line BEMF is simplified properly and the commutation rule for different positions of the rotor is presented. The estimation error of line BEMF caused by the freewheeling current of silent phase is analyzed, and the solution is given. With the phase shift of the low-pass filter considered, a compensation method using “ $60^\circ-\alpha$ ” and “ $120^\circ-\alpha$ ” is studied in this paper to eliminate the error. Finally, the simulation and experimental results show that the rotor-position-detection error is reduced effectively and the motor driven by the accurate commutation signal can work well at low and high speed.

Keywords: line BEMF estimation; sensorless control; phase delay

1. Introduction

The brushless direct current motor (BLDCM), a permanent magnet synchronous motor, has been widely used in varieties of applications including aerospace, industrial automation, hybrid vehicles [1], the military field [2], and household products. A conventional BLDCM control system is mainly formed by a BLDCM, electronic-commutation circuits and position sensors. Hall-effect sensors, electromagnetic variable reluctance sensors, and photoelectric sensors are generally employed to provide the accurate rotor position information for proper commutation of stator currents. However, the use of position sensors not only increases the motor’s size and cost, but also limits the application of the motor where the reliability is of most importance [3–6]. Thus, the use of sensorless control techniques has emerged as required over time, and represents an important research direction with respect to BLDCM control.

Most of the conventional sensorless control strategies of BLDCM are based on back electro-motive force (BEMF) detection, which can be classified into two categories: direct and indirect BEMF detection [7]. The former includes the phase voltage method and terminal voltage method [8–10], which are the most widely used methods, yet these sensorless methods have poor, low-speed performance and require filters to suppress high frequency noise, which may induce large phase shifts to the commutation signals at high speed. Meanwhile, the terminal voltage distortion caused by the diode freewheeling current can make the position detection signal phase advance, deviating from the ideal commutation instant, especially in heavy-load conditions [11]. The indirect BEMF detection

method includes the BEMF integration method [12], a third harmonic of the BEMF method [13], and the freewheeling current method [4]. These methods have their own drawbacks, such as the detection-error accumulation problem at low speeds, large noise interference, and complicated hardware, and as such they are not used widely. In fact, it is important to mention that there is an offset of 30° (electrical) between the BEMF zero-crossing point (ZCP) and the ideal commutation instant. To ensure the correct operation of a motor, this offset should be compensated. In order to achieve a precise sensorless drive, the inherent offset between the BEMF ZCPs and the ideal commutation points, the phase error from filters, the quantization error from the analog-to-digital converter (ADC), errors from circuit components, and voltage spikes caused by the residual current all need to be considered and compensated, and have been discussed in [14–17].

The sensorless drive methods based on the phase BEMF have been studied for many years, while more and more studies have been devoted to the sensorless control based on line BEMF in recent years. Unlike the ZCP of the phase BEMF, the ZCPs of the line BEMF correspond to the commutation points of the motor in one electrical period accurately, guaranteeing better performance in commutation control. On the other hand, the magnitude of the line BEMF is larger than the phase BEMF, which makes it easier to be detected at low rotor speed. Since the line BEMF cannot be extracted directly either, a circuit which constitutes a differential amplifier and a comparator is designed to detect the line voltage in [18]. Nevertheless, this method does not apply to the filter circuit, thus high frequency interference generated by pulse-width modulation (PWM) may cause inaccuracy of commutation. In [19], the line BEMF is reconstructed using the dc bus voltage and three phase duty ratios. The terminal voltage detection circuits are omitted as well, which improves the universality of the hardware. However, this method neglects the phase resistance drop, which may cause a calculation error in the line BEMF, and it does not consider the phase shift of the filter either which will cause a large phase delay at high speed. Bhogineni and Rajagopal presented an analytical prediction method of phase delay caused by the winding resistance drop in the average terminal voltage scheme which is based on the line BEMF detection theory in [20], without an overall error correction method [21].

In most line BEMF-based methods, the line voltage is adopted to exert the commutation signals instead of line-BEMF, which introduces an inherent error since the ZCPs of the two signals are not in the same phase. In this paper, a new sensorless control scheme based on the line-BEMF estimation is proposed. It utilizes the line voltage, the phase current, and other motor parameters to calculate the line BEMF in real time. The commutation error caused by low-pass filters and PWM drive is taken into account, and reliable compensation measures are presented.

2. Principle of Sensorless Control Scheme Based on Line Back Electro-Motive Force Estimation

A control method for a square-wave type surface-mounted three-phase permanent-magnet BLDCM is researched in this paper. In order to analyze the motor and control method theoretically, the mathematical model of the BLDCM is established in a natural coordinate system with the following assumptions:

- (1) The eddy current losses and hysteresis losses are neglected, and the magnetic circuit is always in an unsaturated state;
- (2) The cogging effect of the stator is neglected, and the windings are uniformly arranged on the smooth inner surface of the stator;
- (3) The permanent magnet has no damping effect;
- (4) Armature reaction is neglected;
- (5) All power switch devices have ideal switching characteristics.

The three phases of the BLDCM are defined as phase A, phase B and phase C. According to the electromagnetic characteristics of the BLDCM, the voltage equation is obtained:

$$\begin{bmatrix} u_a \\ u_b \\ u_c \end{bmatrix} = \begin{bmatrix} R_a & 0 & 0 \\ 0 & R_b & 0 \\ 0 & 0 & R_c \end{bmatrix} \begin{bmatrix} i_a \\ i_b \\ i_c \end{bmatrix} + \begin{bmatrix} L_a & L_{ab} & L_{ac} \\ L_{ba} & L_b & L_{bc} \\ L_{ca} & L_{cb} & L_c \end{bmatrix} p \begin{bmatrix} i_a \\ i_b \\ i_c \end{bmatrix} + \begin{bmatrix} e_a \\ e_b \\ e_c \end{bmatrix} \quad (1)$$

where $L_{ab}, L_{ac}, L_{ba}, L_{bc}, L_{ca}$ and L_{cb} are three-phase mutual-inductance, L_a, L_b and L_c are three-phase self-inductance, u_a, u_b and u_c are three-phase voltage, e_a, e_b and e_c are three-phase BEMF, i_a, i_b and i_c are three-phase currents, R_a, R_b and R_c are three-phase resistance, and P is a differential operator. Since the rotor reluctance of the surface-mounted BLDCM does not change with rotor position, three-phase windings are considered symmetrical, by which the following equations are obtained:

$$L_a = L_b = L_c = L, L_{ab} = L_{ac} = L_{ba} = L_{bc} = L_{ca} = L_{cb} = M, R_a = R_b = R_c = R \quad (2)$$

where R, L and M are the resistance, self-inductance and mutual-inductance of the phase winding. In addition, the sum of three-phase currents is zero for the three-phase symmetrical motor, thus the voltage equation can be expressed as:

$$\begin{bmatrix} u_a \\ u_b \\ u_c \end{bmatrix} = \begin{bmatrix} R & 0 & 0 \\ 0 & R & 0 \\ 0 & 0 & R \end{bmatrix} \begin{bmatrix} i_a \\ i_b \\ i_c \end{bmatrix} + \begin{bmatrix} L - M & 0 & 0 \\ 0 & L - M & 0 \\ 0 & 0 & L - M \end{bmatrix} p \begin{bmatrix} i_a \\ i_b \\ i_c \end{bmatrix} + \begin{bmatrix} e_a \\ e_b \\ e_c \end{bmatrix} \quad (3)$$

A general BLDCM with three-phase stator windings is driven by a half-bridge inverter which constitutes of six switches. Figure 1 shows the equivalent circuit of a star wound motor based on the voltage Equation (3) and the three-phase inverter topology.

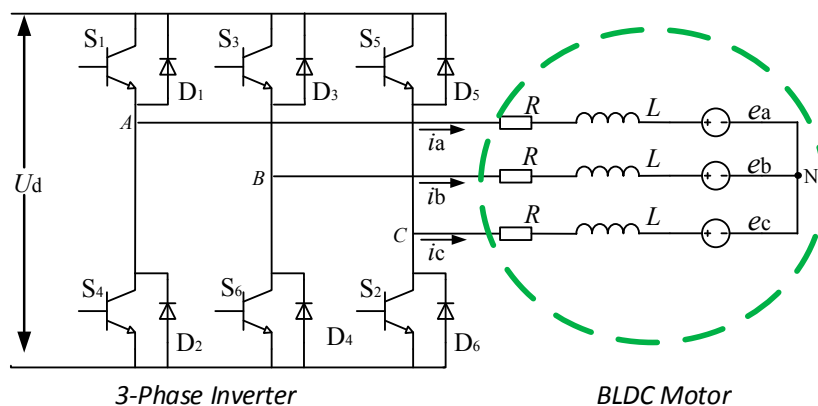


Figure 1. A brushless direct current motor (BLDCM) and a three-phase inverter block diagram.

The proposed sensorless control scheme utilizes the line BEMF instead of the phase BEMF for BLDCM drive. The relationship between the line BEMF and commutation points of the stator current is shown in Figure 2. Similar to the phase BEMF, the line BEMF is also trapezoidal. As shown in Figure 2, the six ZCPs of the line BEMF e_{ac}, e_{ba} and e_{cb} : $\pi/3, 2\pi/3, \pi, 4\pi/3, 5\pi/3$ and $2\pi(0)$, correspond to the six commutation points. Through this relationship, the commutation can be realized by detecting the line BEMF.

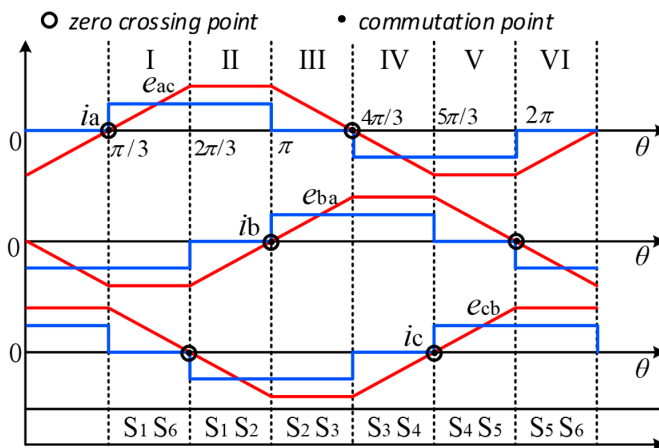


Figure 2. Line back electro-motive force (BEMF) and stator current of each phase.

Since the line BEMF cannot be extracted directly, a formula is needed for estimating the line BEMF using the electrical parameters that can be detected. Assuming that the three-phase windings are symmetrical and the stator resistance and inductance of the three-phase windings are equal, the line voltage equations of the BLDCM can be expressed as:

$$\begin{aligned}
 e_{ac} &= u_{ac} - R(i_a - i_c) - (L - M) \frac{d}{dt}(i_a - i_c) \\
 e_{ba} &= u_{ba} - R(i_b - i_a) - (L - M) \frac{d}{dt}(i_b - i_a) \\
 e_{cb} &= u_{cb} - R(i_c - i_b) - (L - M) \frac{d}{dt}(i_c - i_b)
 \end{aligned}
 \tag{4}$$

where e_{ac} , e_{ba} and e_{cb} are the line BEMF, and u_{ac} , u_{ba} and u_{cb} are the line voltages.

It is indicated from Formula (4) that the value of line BEMF is only related to the line voltage, phase current and motor parameters. However, the value of the stator inductance is difficult to detect in real time which will change along with the rotor position of the motor. Therefore, Formula (4) needs to be simplified.

When the motor rotates clockwise, the line BEMF e_{ac} is taken as an example. Firstly, during the non-commutation periods ($d(i_a - i_c)/dt = 0$), the differential terms of Equation (4) are equal to zero, so the inductances of L and M have no effect on the detection of ZCPs. At the commutation instant ($d(i_a - i_c)/dt \neq 0$), the voltage spike in detected line voltage caused by inductances is consistent with the polarity of the line BEMF, which has no effect on the detection of ZCPs. Therefore, the differential terms in Equation (4) are neglected because they have no effect on the detection of ZCPs. Secondly, before the commutation instant, since phase A is in a non-conduction state, the corresponding current i_a is equal to zero. Similarly, e_{ba} and e_{cb} can be simplified as above, and the final estimation formulas of the line BEMF can be described as:

$$\begin{aligned}
 e_{ac} &= u_{ac} + Ri_c \\
 e_{ba} &= u_{ba} + Ri_a \\
 e_{cb} &= u_{cb} + Ri_b
 \end{aligned}
 \tag{5}$$

When the motor rotates anticlockwise, the simplified principle of the line BEMF is the same as above but only the float phase is different before the commutation instant. The simplified formulas can be described as:

$$\begin{aligned}
 e_{ac} &= u_{ac} - Ri_a \\
 e_{ba} &= u_{ba} - Ri_b \\
 e_{cb} &= u_{cb} - Ri_c
 \end{aligned}
 \tag{6}$$

The simplified formula is used to estimate the line BEMF, and then the calculated line BEMF is converted into digital position signals H_{AC} , H_{BA} and H_{CB} , as shown in Figure 3. The corresponding digital position signals remain at high level when the value of the line BEMF is positive, and stay at a low level when the value is negative.

The same as the Hall position signals, these three digital position signals have a 120-electrical-degree relative offset from each other, and the commutation action can be simply triggered by using these signals. When any one of the digital position signals undergoes a forward or a backward transition, it is indicated that the commutation needs to be performed. Then, with the level of the other two signals judged and the Table 1 further checked, the rotor position and the corresponding commutation control strategy for the BLDCM can be obtained.

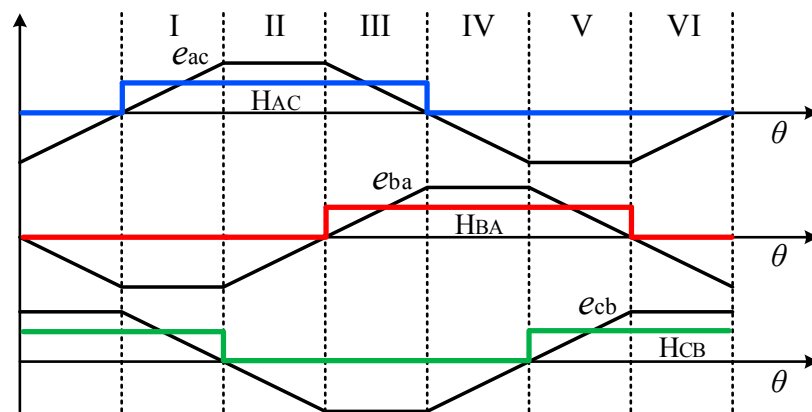


Figure 3. Line BEMF and the digital position signal. H_{AC} , H_{BA} and H_{CB} : digital position signals.

Table 1. Commutation control strategy for BLDCM.

Rotor Position	H_{AC}	H_{BA}	H_{CB}	Active Phase	Active Switches
VI→I	↗	0	1	+A, -B	S_1, S_6
I→II	1	0	↘	+A, -C	S_1, S_2
II→III	1	↗	0	+B, -C	S_3, S_2
III→IV	↘	1	0	+B, -A	S_3, S_4
IV→V	0	1	↗	+C, -A	S_5, S_4
V→VI	0	↘	1	+C, -B	S_5, S_6

Note: 1 represents the high level, 0 represents the low level, ↗ represents the forward transition, and ↘ represents the backward transition.

3. Analyses and Compensation of Commutation Control Error

3.1. Phase-Shift Error Caused by the Low-Pass Filter

The high frequency noise in the line voltage, the phase current caused by the PWM drive and other high frequency interference may cause the pseudo zero-crossings of the calculated line BEMF. Therefore, the low-pass filter needs to be used to filter out the high frequency noise, but it will result in the phase delay of the detected voltage and current, which will introduce the commutation delay at last. Figure 4 shows the circuit of the required low-pass filter.

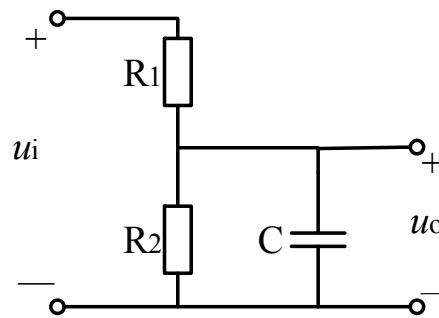


Figure 4. Circuit of the low-pass filter.

The amplitude-frequency characteristic of the first-order low-pass filter circuit composed of R_1 , R_2 and C is:

$$|A(\omega)| = \frac{R_2}{\sqrt{(R_1 + R_2)^2 + (R_1 R_2 C \omega)^2}} \quad (7)$$

The phase shift angle is:

$$\alpha = \arctan\left(\frac{R_1 R_2 C \omega}{R_1 + R_2}\right) \quad (8)$$

As can be seen from the above formula, the phase shift angle increases along with the increase of the motor speed, and ranges from 0 to 90 degrees. When the speed is higher than a certain value, the angle will exceed 60 degrees. In this circumstance, the ZCPs of the calculated line BEMF will have an offset that is more than 60° from the ideal commutation points, which will make the ZCPs lag behind the next commutation point. Therefore a proper commutation-compensation method is required to eliminate the error caused by the filter at low and high speed, respectively. The compensation method is based on the assumption that, during the period $60^\circ - \alpha$ or $120^\circ - \alpha$, the speed does not change, though the actual change of speed does have effect on the sensing accuracy. At low speed, the commutation time interval is too large to tolerate the speed changes, so the compensation method is not applicable for low speed operations. As the phase shift angle α is small at low speed, the commutation point can be calculated directly. The compensation method of “ $60^\circ - \alpha$ ” and “ $120^\circ - \alpha$ ” is used when the speed is high enough so the speed change error is negligible.

The resistance and capacitance, which will change with the temperature, also have effect on the calculation of phase shift angle. On the one hand, the computational accuracy can be improved through utilizing the temperature curves of resistance and capacitance which can be obtained by theoretical model or experiments. On the other hand, the error caused by temperature can be reduced by using high precision resistance and capacitance with small temperature coefficient.

When the motor speed is low, the phase shift angle is less than 60° and the compensation strategy is working under the $60^\circ - \alpha$ mode. The scheme of the $60^\circ - \alpha$ mode compensation strategy is shown in Figure 5. In this picture, e_{ac} , e_{ba} and e_{cb} are the ideal line BEMF, while e_{ac}' , e_{ba}' and e_{cb}' are the filtered line BEMF. The symbol α and γ stand for the phase-shift angle of the filter and the compensation angle, respectively. Taking the ideal commutation point Z (the ZCP of e_{cb}) as an example, after filtering, this point is delayed to point P (the ZCP of e_{cb}'), which is before the next ideal commutation point C (the ZCP of e_{ba}). In order to realize the accurate commutation, point P is required to be moved backward by $60^\circ - \alpha$ electrical degree to point C.

After the $60^\circ - \alpha$ phase compensation, the calculated line BEMF signal is delayed by one rotor interval, and the ideal commutation points corresponding to the six ZCPs of the line BEMF also change, which is shown in Figure 6. The commutation control strategy in the $60^\circ - \alpha$ mode is shown in Table 2.

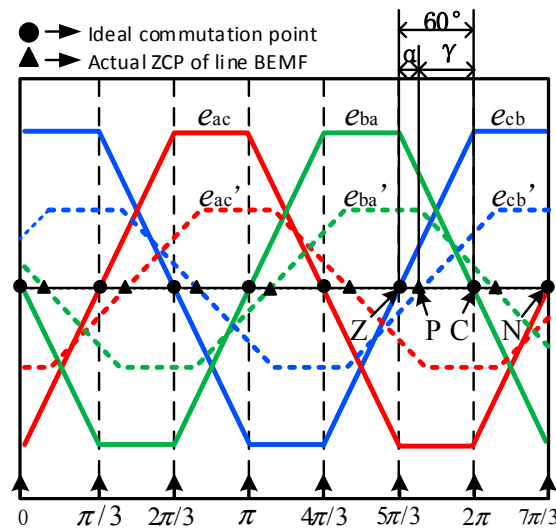


Figure 5. Scheme of 60°-α mode. ZCP: zero-crossing point.

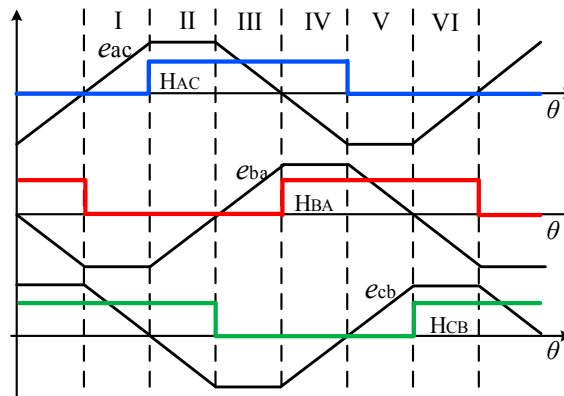


Figure 6. Digital position signals in the 60°-α mode.

Table 2. Commutation control strategy in the 60°-α compensation mode.

Rotor Position	H _{AC}	H _{BA}	H _{CB}	Active Phase	Active Switches
VI→I	0	↘	1	+A, -B	S ₁ , S ₆
I→II	↗	0	1	+A, -C	S ₁ , S ₂
II→III	1	0	↘	+B, -C	S ₃ , S ₂
III→IV	1	↗	0	+B, -A	S ₃ , S ₄
IV→V	↘	1	0	+C, -A	S ₅ , S ₄
V→VI	0	1	↗	+C, -B	S ₅ , S ₆

For the low-speed BLDCM, the 60°-α mode can meet the need of the phase compensation, but for the motors with a large number of pole pairs or working at high speed, the phase-shift angle of the low-pass filter will exceed 60 degrees, in which circumstance the 60°-α compensation mode is invalid and the 120°-α compensation mode needs to be performed. The scheme of the 120°-α compensation mode is shown in Figure 7. In this case, α is larger than 60°, thus the ideal commutation point Z is delayed to point P which lags behind the next ideal commutation point C. A 120°-α compensation-phase angle is needed to be applied to point P, which means the ZCPs of the filtered line BEMF will be at the same phase with the ideal commutation points again. The digital position signals and the commutation control strategy in the 120°-α mode are shown in Figure 8 and Table 3, respectively.

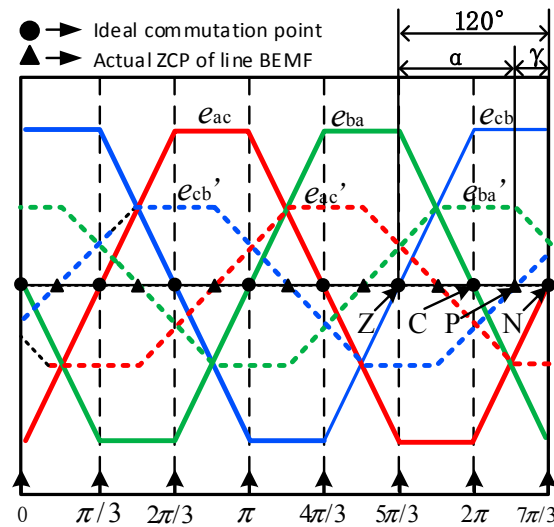


Figure 7. Scheme of 120°-α mode.

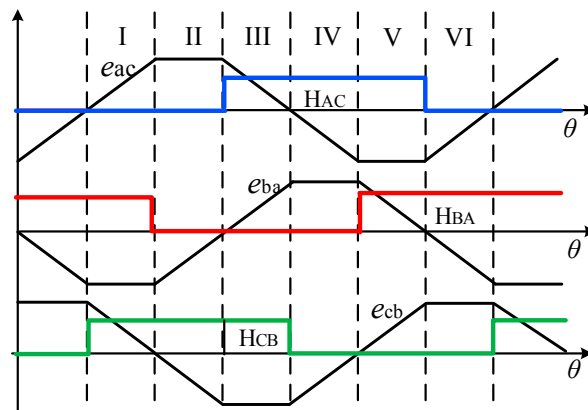


Figure 8. Digital position signals in the 120°-α mode.

Table 3. Commutation control strategy in the 120°-α compensation mode.

Rotor Position	H _{AC}	H _{BA}	H _{CB}	Active Phase	Active Switches
VI→I	0	1	↗	+A, -B	S ₁ , S ₆
I→II	0	↘	1	+A, -C	S ₁ , S ₂
II→III	↗	0	1	+B, -C	S ₃ , S ₂
III→IV	1	0	↘	+B, -A	S ₃ , S ₄
IV→V	0	↗	0	+C, -A	S ₅ , S ₄
V→VI	↘	1	0	+C, -B	S ₅ , S ₆

Through this compensation strategy, the commutation error caused by the low-pass filter can be reduced efficiently. At low speed, the 60°-α compensation mode is utilized, while at the high speed, the commutation is switched to the 120°-α compensation mode. The speed switching threshold needs to be calculated based on the parameters of the filter and motor, which can be expressed as:

$$n^* = \frac{30\sqrt{3}(R_1 + R_2)}{\pi R_1 R_2 C p} \tag{9}$$

3.2. Commutation Error Due to the PWM Drive

The 120° conduction mode, where the current flows through only two phase windings at any time, is selected as the commutation mode of the BLDCM. There are six commonly used PWM-control methods for this conduction mode: PWM-ON, ON-PWM, H-PWM-L-ON, H-ON-L-PWM, H-PWM-L-PWM and PWM-ON-PWM, as shown in Figure 9.

For the PWM-ON and ON-PWM control methods, it is shown in Figure 9a,b that the conduction region (120°) is divided into two equal intervals (60°), and the bridges of the inverters are controlled by the PWM signal or kept in conducting state in different intervals. H-PWM-L-ON method controls the upper bridges with PWM signals and the lower bridges are kept in a conducting state. The H-ON-L-PWM method controls the lower bridges with PWM signals and the upper bridges are kept in conducting state. All the bridges are controlled by PWM signals in H-PWM-L-PWM method. The PWM-ON-PWM method utilizes the PWM control during the first 30° interval and the last 30° interval, while the bridges are kept in conducting state during the middle 60° interval.

PWM-ON method is taken as an example to analyze the commutation error caused by the PWM drive. When the BLDCM operates in the 120° conduction mode, it is desired that the current flows through only two phase windings at any time, which means there are no current flows in the unexcited phase. In fact, due to the use of PWM chopper control, the non-conduction phase windings also have current passing by, as shown in Figure 10. Take A-phase current as an example, there are four non-conduction intervals 0 to $\pi/6$, $5/6\pi$ to π , π to $7/6\pi$ and $11/6\pi$ to 2π in one electrical period. Compared with the normal operating current, the non-conduction-phase current, whose amplitude is small and presents a pulsating form, flows in the winding without flowing through the DC bus, which makes it difficult to be detected and suppressed.

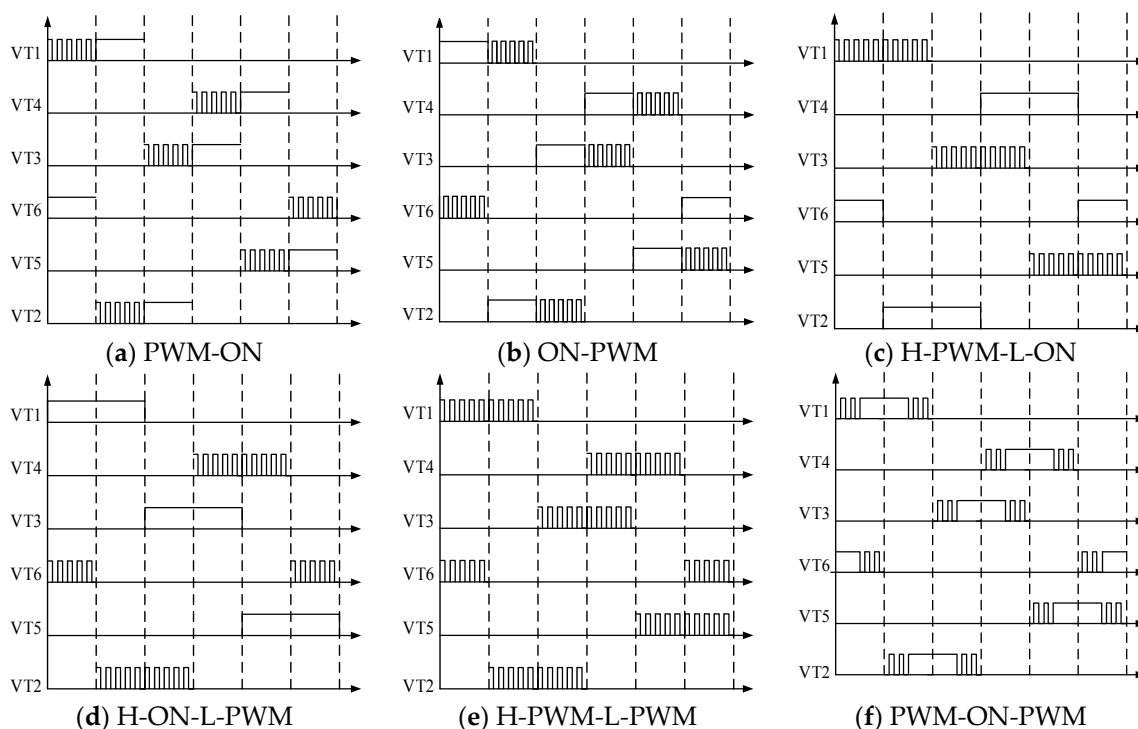


Figure 9. Six commonly used PWM-control methods. PWM: pulse-width modulation.

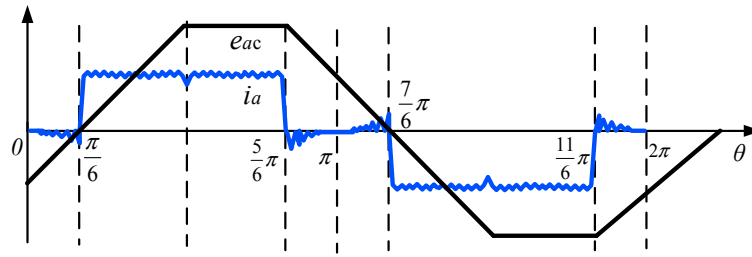


Figure 10. Non-conduction intervals of the A-phase current.

According to the simplified conditions of the line BEMF calculation proposed in Section 2, it is required that there is no current flowing in the unused phase before it is conducted, in other words, the freewheeling current should not exist in the 0-to- $\pi/6$ and π -to- $7/6\pi$ intervals. The effect of freewheeling current of the unused phase on the line BEMF calculation is analyzed in detail below. The freewheeling circuit is shown by the dotted line in Figure 11.

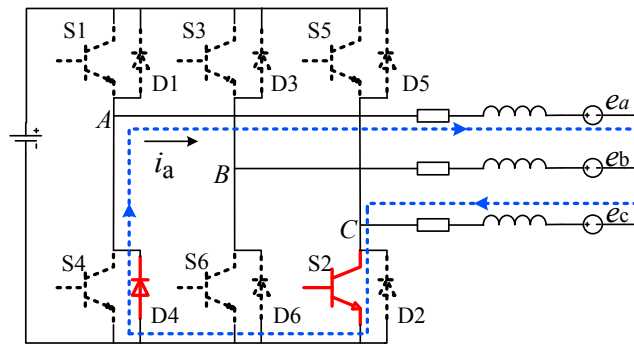


Figure 11. The freewheeling circuit in the π -to- $7/6\pi$ non-conduction intervals of A phase.

The A phase is in the π -to- $7/6\pi$ non-conduction interval under the PWM-ON drive. The freewheeling is performed through the power switch S2 and diode D4, and the terminal point A is connected to the power ground, thus terminal voltage U_a is 0 V. When the inverter switch S3, which is on the upper bridge arm of B phase, is off (PWM_OFF), the three-phase voltage is zero, and the phase BEMF $e_b = -e_c = E$, and $e_a < 0$. The current equation of the BLDCM can be obtained as shown in Equation (10):

$$\frac{e_a + U_N}{Z} + \frac{e_b + U_N}{Z} + \frac{e_c + U_N}{Z} = 0 \tag{10}$$

where U_N is the neutral point voltage, and Z is the impedance of each phase. By Equation (10), $U_N = -1/3e_a$. Therefore, the expression of the voltage drop on the A phase windings is $U_{axf} = -(e_a + U_N) = -2/3e_a$.

Since $U_{axf} > 0$, by $Ri_A + L \frac{di_a}{dt} = U_{axf}$, the freewheeling current can be expressed as:

$$i_{a_off} = \frac{U_{axf}}{R} + c_1 e^{-\frac{R}{L}t} = -\frac{2e_a}{3R} (1 - e^{-\frac{R}{L}t}) \tag{11}$$

In a similar way, when the inverter switch S3 is on (PWM_ON), the current equation of the BLDCM is:

$$\frac{e_a + U_N}{Z} + \frac{e_b + U_N - U_d}{Z} + \frac{e_c + U_N}{Z} = 0 \tag{12}$$

where U_d is the DC bus voltage. The neutral point voltage is obtained: $U_N = 1/3U_d - 1/3e_a$ and the voltage drop on the A phase windings is $U_{axn} = -(e_a + U_N) = -1/3U_d - 2/3e_a$. Therefore, the freewheeling current of A phase can be expressed as:

$$i_{a_on} = \frac{U_{axn}}{R} + c_1 e^{-\frac{R}{L}t} = -\frac{U_d + 2e_a}{3R} (1 - e^{-\frac{R}{L}t}) \tag{13}$$

According to the above derivation, we can get the voltage and current waveform of A phase winding in the π -to- $7/6\pi$ non-conduction interval, as shown in Figure 12.

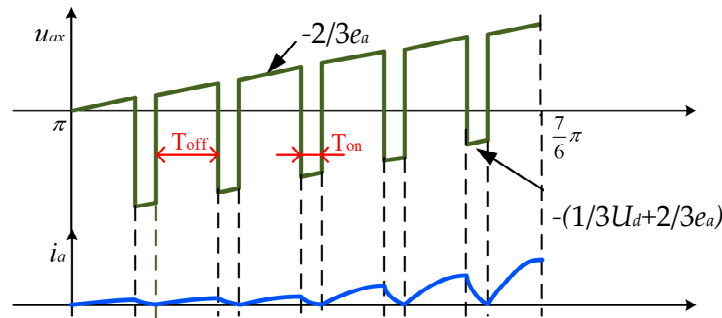


Figure 12. Voltage and current waveform of the inactive phase winding. T_{on} and T_{off} represent the turn-on and turn-off time of a inverter switch in one chopper period.

Where T_{on} and T_{off} represent the turn-on and turn-off time of a inverter switch in one chopper period. As can be seen from Figure 12, during the T_{off} interval, the inactive phase current continues to increase, and the closer it is to $7/6\pi$, the greater the current amplitude is. During the T_{on} interval, the current continues to decrease. Similarly, the expression of non-conduction phase current in the 0-to- $\pi/6$ interval can be deduced, and the result is consistent with the expression in the π -to- $7/6\pi$ interval. Therefore, the maximum value of the non-conduction phase current is generated at $\pi/6$ and $7/6\pi$, which is the commutation point of the stator current. The expression of the maximum value can be expressed as:

$$I_{zmax} = -\frac{K_e \omega}{R} (1 - e^{-\frac{R}{L}T_{off}}) \tag{14}$$

where K_e stands for the BEMF constant. The calculation error of the line BEMF at the commutation instant is:

$$\Delta u_{ac} = -K_e \omega (1 - e^{-\frac{R}{L}T_{off}}) \tag{15}$$

Such an error makes the calculated line BEMF less than the actual line BEMF at the commutation point, which results in a commutation delay of the BLDCM. It is important to choose a proper PWM method to eliminate the error caused by the freewheeling of the inactive phase.

Based on the above analysis, the freewheeling currents in unexcited phase caused by these PWM methods are analyzed, as shown in Table 4. It is shown that both the PWM-ON-PWM and H-PWM-L-PWM method can eliminate the diode freewheeling currents in the unexcited phase completely, which theoretically can reduce the calculation error of the line BEMF. With switching losses considered, the PWM-ON-PWM method is preferred.

Table 4. Freewheeling currents in unexcited phase caused by different PWM methods.

	0~ $\pi/6$	5/6 π ~ π	π ~7/6 π	11/6 π ~2 π
PWM-ON	√(-)	×	√(+)	×
ON-PWM	×	√(-)	×	√(+)
H-PWM-L-ON	×	×	√(+)	√(+)
H-ON-L-PWM	√(-)	√(-)	×	×
PWM-ON-PWM	×	×	×	×
H-PWM-L-PWM	×	×	×	×

Where √ represents that the freewheeling current exists, (-) represents that the current direction is negative, (+) represents that the current direction is positive, and × represents that there is no freewheeling current.

4. Simulation and Experiment Results

The simulation and experiment are carried out to verify the effectiveness and control precision of the proposed BLDCM sensorless control method. The major parameters applied in this paper are listed in Table 5.

Table 5. Motor parameters.

Parameters	Value	Parameters	Value
Rated direct current (DC) voltage	3	Back electro-motive force (EMF) Constant	0.048 V/(rad/s)
Rated speed, n	1500 rpm	Rotor inertia, J	0.08 kg·m ²
Rated Power	1 kW	Filter resistance, R_1	5.6 M Ω
Number of pole pairs, p	4	Filter resistance, R_2	27 k Ω
Phase resistance, R	0.94 Ω	Filter capacitance, C	94 nF
Phase inductance, L	1.43 mH	Pulse-width modulation (PWM) frequency	20 kHz
Mutual inductance, M	0.41 mH		

The block diagram of the sensorless control system based on the line BEMF estimation is shown in Figure 13, which consists of a speed loop proportional-integral (PI) controller, a current loop PI controller, a PWM generator block, a commutation control block, ZCPs of the line BEMF detection block, and a phase compensation algorithm block, etc. Compared with the conventional BLDC sensorless control system, a line BEMF estimation module and a closed-loop phase error compensation module are applied.

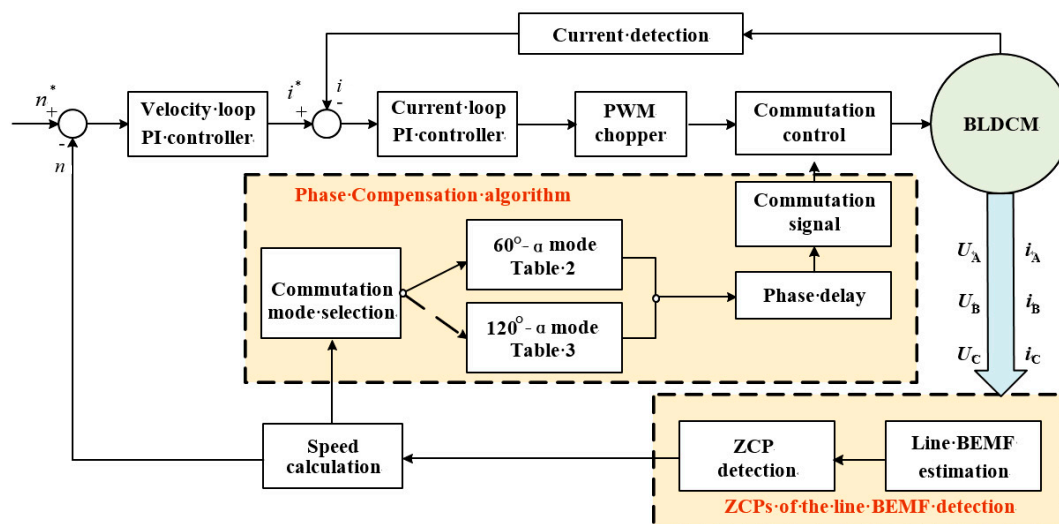


Figure 13. Block diagram of a BLDCM control system.

4.1. Simulation Results

4.1.1. Phase Compensation Strategy Simulation

The proposed method is simulated using MATLAB/SIMULINK software. The simulation model is mainly composed of a BLDCM module, a three-phase voltage inverter module, a low-pass filter module, line BEMF module, a PI module and a PWM-ON-PWM generating module. The PWM chopping frequency and the system sampling frequency under simulation are 20 kHz and 100 kHz, respectively. By calculating Equation (6), the speed switching threshold is 1672 rpm. In order to verify the phase compensation strategy, the simulation is performed under 500 rpm and 3000 rpm.

The simulation results of ideal and estimated line BEMF waveform at the speed of 500 rpm and 3000 rpm are shown in Figure 14. Obviously, there is a phase delay on the estimated line BEMF, which is 30.2 degree under 500 rpm and 72.5 degree under 3000 rpm.

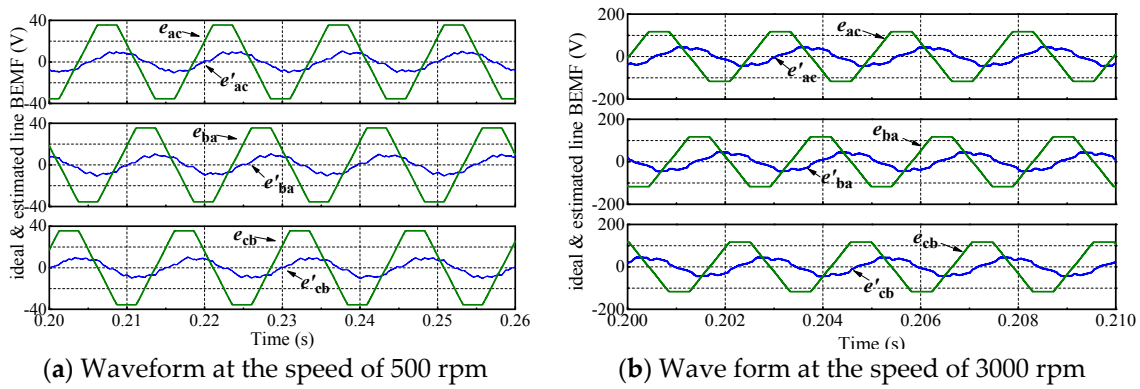


Figure 14. Ideal and estimated line BEMF.

Using the $60^\circ\text{-}\alpha$ phase compensation method, the digital position signals are shown in Figure 15, in which the digital position signals are lagged by 60 degrees to the Hall signal after compensation. Through the commutation control method presented in Table 2, the commutation instant of stator current matches the ideal commutation position represented by the Hall signal.

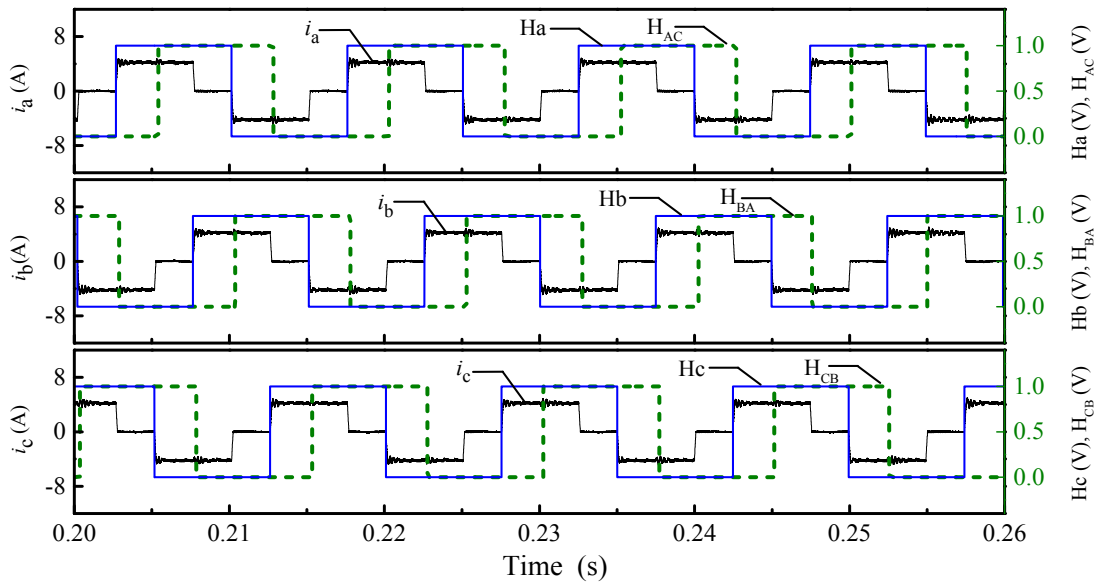


Figure 15. Stator current waveform, Hall signal and compensated digital position signal ($n = 500$ rpm).

As shown in Figure 16, the compensation method is switched to $120^\circ\text{-}\alpha$ mode, and meanwhile, digital position signals are delayed 120 degrees from the Hall signals. The current commutation is completed accurately by the strategy shown in Table 3. The simulation results verify the effectiveness of the proposed commutation compensation method.

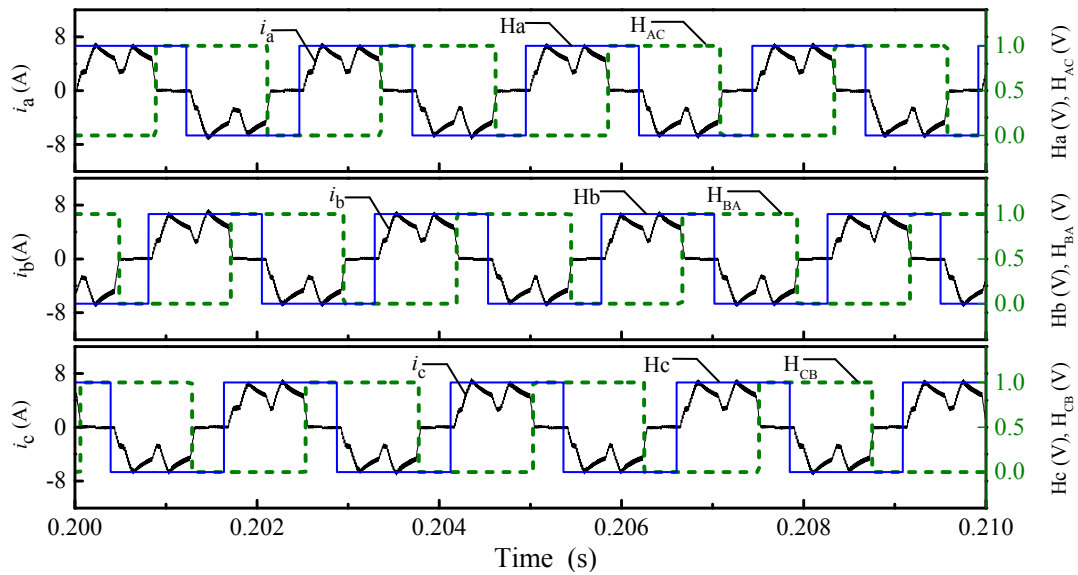


Figure 16. Stator current waveform, Hall signal and compensated digital position signal ($n = 3000$ rpm).

4.1.2. Commutation Error Elimination Simulation

The performance of the chosen method PWM-ON-PWM is compared with that of the PWM-ON method through simulation. The bus voltage of the system is 300 V and the PWM chopping frequency is 16 kHz. Figure 17 shows the phase-A current waveforms of different methods under the speed of 1200 r/min and the torque of 1.5 N·m. When the phase-A current change from zero to positive or negative, the freewheeling current of the PWM-ON method is larger than that of the PWM-ON-PWM method.

It is indicated that the freewheeling current of the PWM-ON-PWM method is less than that of the PWM-ON method.

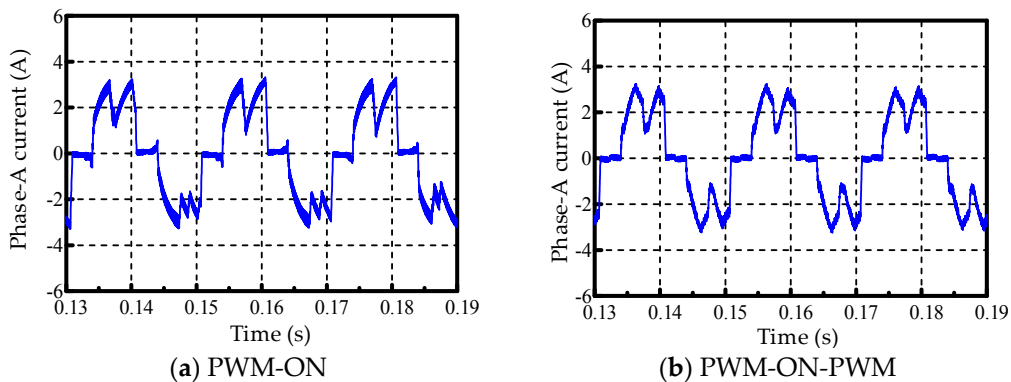


Figure 17. Phase-A current waveforms of different methods.

With the speed fixed at 1500 r/min, the relationship between freewheeling-current amplitude of non-conduction phase and frequency is shown in Figure 18.

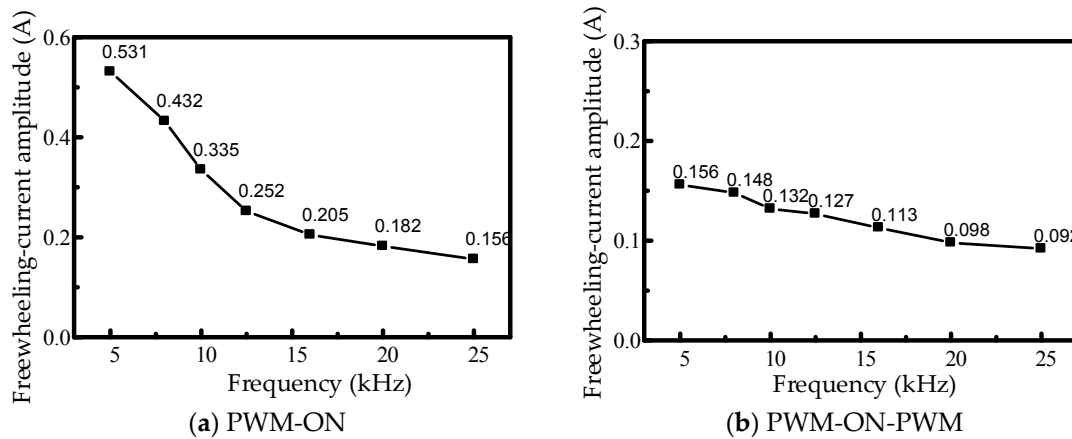


Figure 18. Relationship between freewheeling-current amplitude of non-conduction phase and frequency.

It is illustrated that the freewheeling-current amplitudes of both methods decrease with the increase of frequency. However, the change range of the PWM-ON method is larger than that of the PWM-ON-PWM method and the freewheeling-current amplitude of the PWM-ON-PWM method is much smaller, which means that the PWM-ON-PWM method is better at eliminating the freewheeling current.

With the frequency fixed at 16 kHz, the relationship between freewheeling-current amplitude of non-conduction phase and speed is shown in Figure 19. It is indicated that the freewheeling-current amplitude of the PWM-ON method increases with speed, while the freewheeling-current amplitude of the PWM-ON-PWM method increases first, and then almost stays the same after the speed of 1500 r/min.

Afterwards, electrical angle error is calculated as below:

$$\Delta\theta = \frac{\Delta t}{T_e} \times 360^\circ = \frac{\Delta t}{60/np} \times 360^\circ = 6np\Delta t$$

where Δt is the difference between current commutation time and Hall signal commutation time. The calculated result is shown in Figure 20, from which it can be seen that the electrical angle error of the PWM-ON-PWM method is much less than that of the PWM-ON method. The electrical angle error of the PWM-ON-PWM method stabilizes at 2.6° with the increase of speed, demonstrating the good high-speed performance of the system.

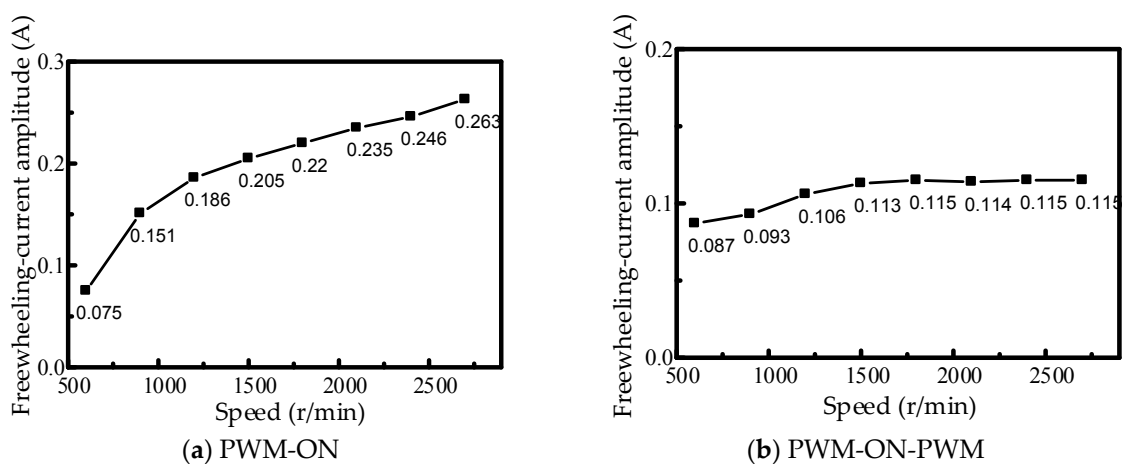


Figure 19. Relationship between freewheeling-current amplitude of non-conduction phase and speed.

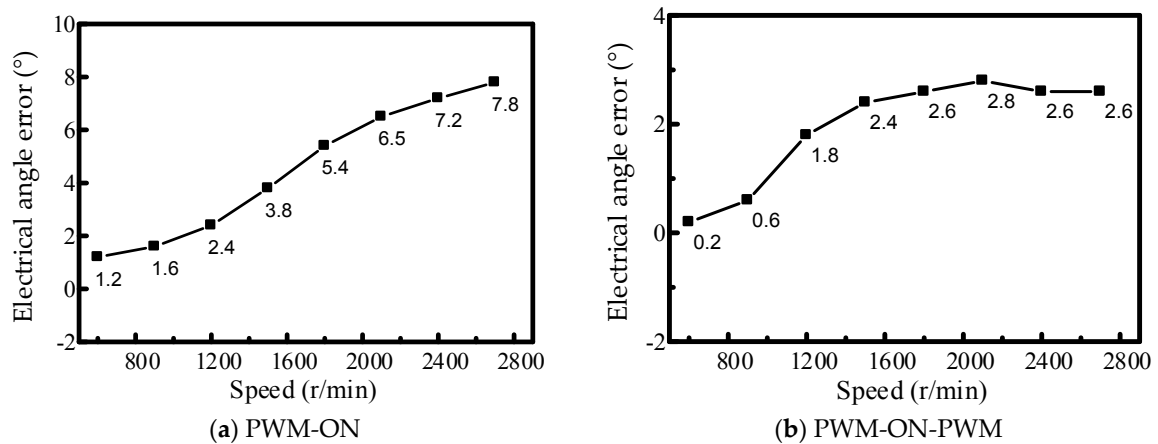


Figure 20. Electrical angle error of different methods.

According to the above analysis, the PWM-ON-PWM method is selected for the control system to eliminate the commutation error, and the system performance can be further improved by promoting the chopping frequency of PWM-ON-PWM method properly.

4.2. Experiment Results

With experimental platform set up, experiment is carried out to verify the performance of the proposed control method. The experimental platform is composed of the BLDCM, controller and dynamometer, as shown in Figure 21. The bus voltage of the inverter is from 0 to 180 V. The controller (HVMotorCtrl + PfcKit from Texas Instruments Company, Dallas, TX, USA) is composed of a drive unit and control unit, as shown in Figure 22.

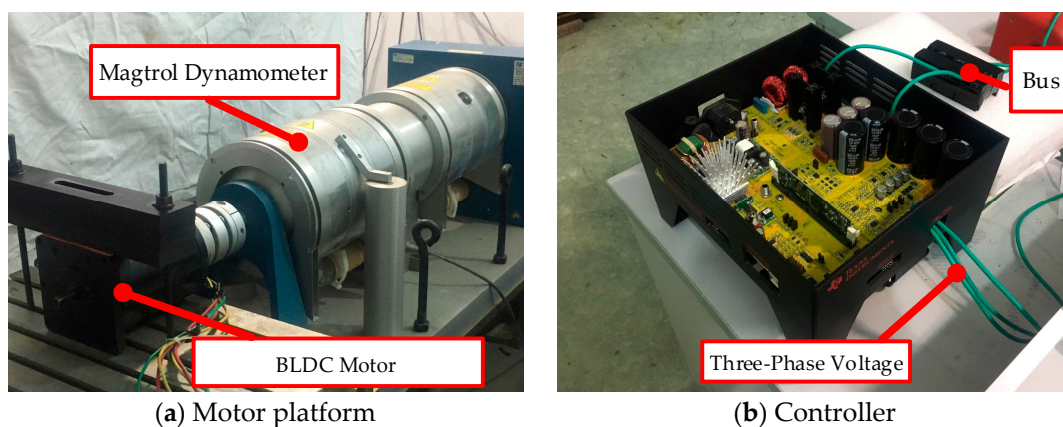


Figure 21. Experimental platform.

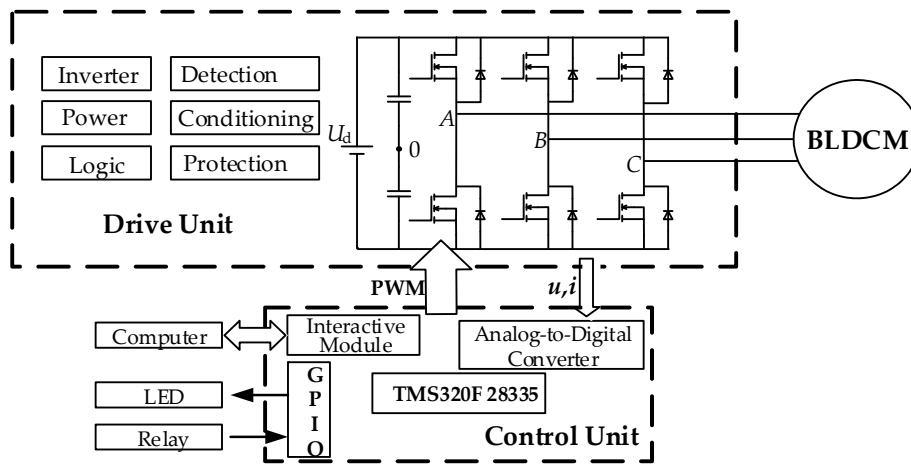


Figure 22. The structure of the controller. GPIO: general purpose input/output. LED: light-emitting diode.

When the BLDCM runs stably with the proposed control system, the PWM output and the three-phase voltages of the system are detected. Figure 23 shows the PWM output waveform of the PWM-ON-PWM method. Figure 24 illustrates the waveform of three-phase voltage, and it is indicated that the three-phase voltages are equal-amplitude trapezoidal waves and the phase shift between each other is 120° , which is consistent with the theory.

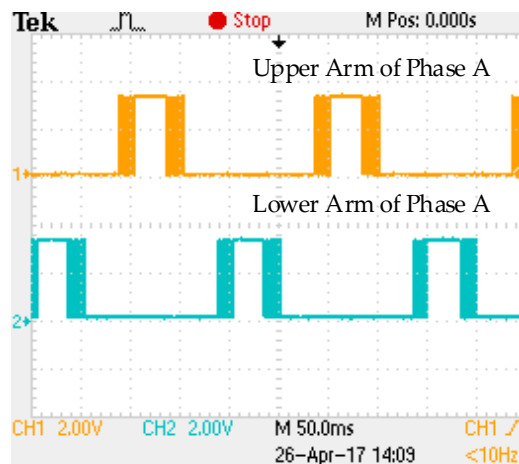


Figure 23. The waveform of PWM output.

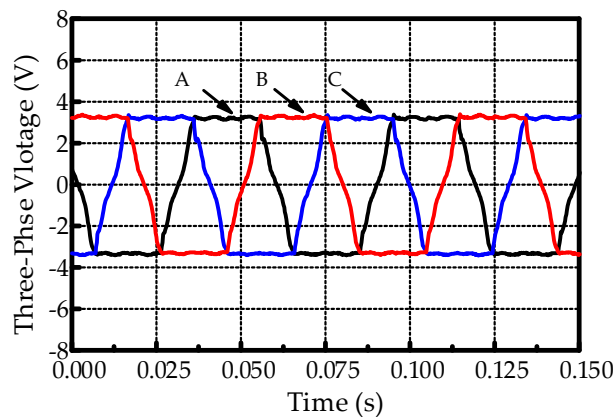


Figure 24. The waveform of three-phase voltage.

With the motor speeds set at 300 r/min and 3000 r/min, $60^\circ\text{-}\alpha$ and $120^\circ\text{-}\alpha$ phase compensation methods are tested, respectively, and the commutation signals are compared with Hall signals to verify the validity of the proposed methods, as shown in Figures 25 and 26. It is indicated that the commutation error of the two methods are 2.16° and 6.26° , respectively.

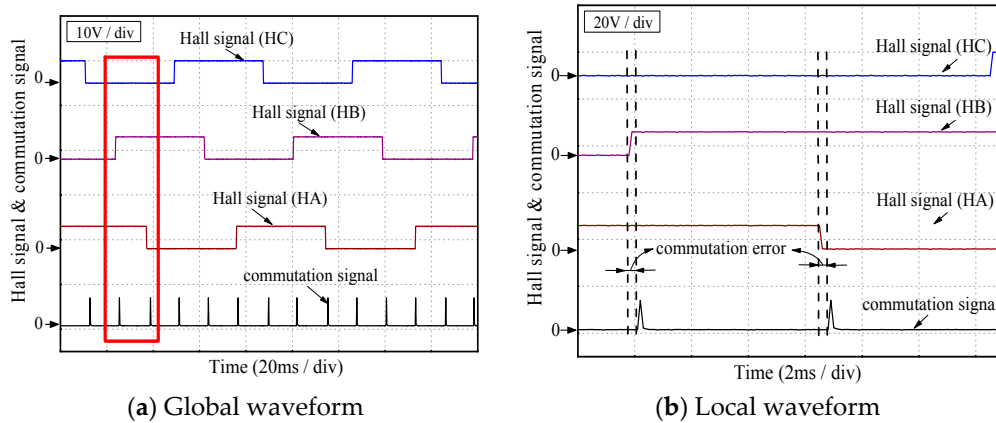


Figure 25. Waveforms of the commutation signal and Hall signals (300 r/min).

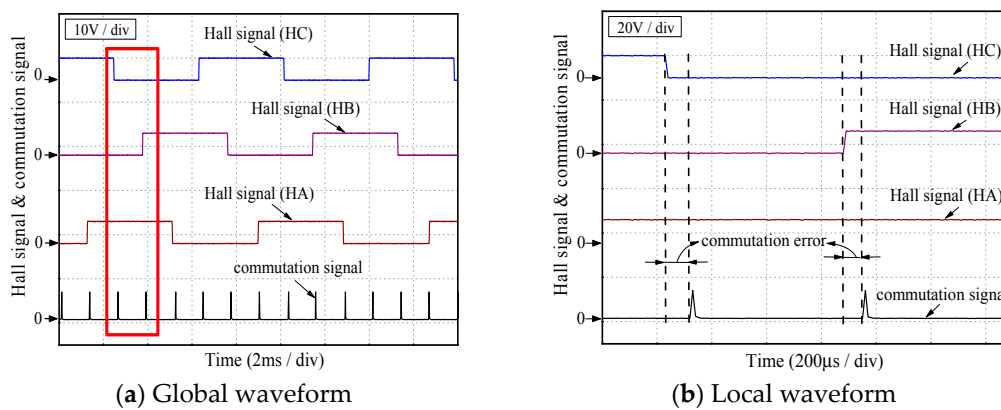


Figure 26. Waveforms of the commutation signal and Hall signals (3000 r/min).

Afterwards, the commutation errors at different speeds are examined, as shown in Figure 27. It is illustrated that the commutation error, which is composed of algorithm error and hardware error, shows an increase trend with the increasing speed and reaches the highest at speed switching threshold. During the low-speed operation, $60^\circ\text{-}\alpha$ phase compensation method is utilized and the error is less than 6° ; while during the high-speed operation, the error of $120^\circ\text{-}\alpha$ phase compensation method is less than 7° . In conclusion, the proposed method can achieve accurate commutation.

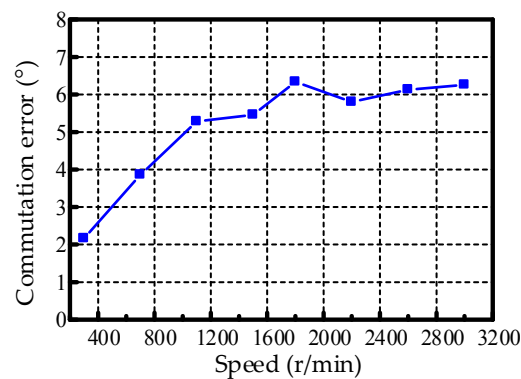


Figure 27. Commutation errors at different speeds.

5. Conclusions

- (1) A novel sensorless control strategy based on the line-BEMF estimation is proposed for the BLDCM, with the commutation error caused by low-pass filters and PWM drive considered.
- (2) The $60^\circ\text{-}\alpha$ and $120^\circ\text{-}\alpha$ mode compensation strategies are proposed to eliminate the error caused by the filter at low and high speed. The ZCPs of the filtered line BEMF are at the same phase with ideal commutation points in the use of the proposed strategies.
- (3) PWM-ON-PWM method is utilized to avoid the freewheeling current of the non-conduction phase, by which the commutation error is eliminated.
- (4) Simulation and experiment are carried out, and it is proved that the BLDCM is able to operate stably with the proposed control method. The commutation errors at low and high speed are kept below 6° and 7° , respectively.

Acknowledgments: This work was supported in part by National Key R&D Program of China under Project 2017YFB0203603, in part by National Natural Science Foundation of China under Project 51325701, 51521003, 51377033 and 51407042, in part by China Postdoctoral Science Foundation, and in part by Self-Planned Task (No. 201504B) of State Key Laboratory of Robotics and System (HIT).

Author Contributions: Chengde Tong, Baige Zhao and Ping Zheng conceived, designed and performed the analytical analysis of the control method. Mingqiao Wang, Baige Zhao and Zuosheng Yin carried out the experiments and wrote the paper.

Conflicts of Interest: The authors declare no conflict of interest.

References

1. Naidu, M.; Nehl, T.W.; Gopalakrishnan, S.; Wurth, L. Keeping cool while saving space and money: A semi-integrated, sensorless PM brushless drive for a 42-v automotive HVAC compressor. *IEEE Ind. Appl. Mag.* **2005**, *11*, 20–28. [[CrossRef](#)]
2. Hubik, V.; Sveda, M.; Singule, V. On the Development of BLDC Motor Control Run-up Algorithms for Aerospace Application. In Proceedings of the 13th Power Electronics and Motion Control Conference (EPE-PEMC 2008), Poznan, Poland, 1–3 September 2008; pp. 1620–1624.
3. Kim, T.; Lee, H.W.; Ehsani, M. Position sensorless brushless DC motor/ generator drives: Review and future trends. *IET Electr. Power Appl.* **2007**, *1*, 557–564. [[CrossRef](#)]
4. Ogasawara, S.; Akagi, H. An approach to position sensorless drive for brushless DC motors. *IEEE Trans. Ind. Appl.* **1991**, *27*, 928–933. [[CrossRef](#)]
5. Acarnley, P.P.; Watson, J.F. Review of position-sensorless operation of brushless permanent-magnet machines. *IEEE Trans. Ind. Electron.* **2006**, *53*, 352–362. [[CrossRef](#)]
6. Johnson, J.P.; Ehsani, M.; Guzelgunler, Y. Review of Sensorless Method for Brushless DC. In Proceedings of the Thirty-Fourth IAS Annual Meeting, Conference Record of the 1999 IEEE Industry Applications Conference, Phoenix, AZ, USA, 3–7 October 1999; Volume 1, pp. 143–150.
7. Vinatha, U.; Pola, S.; Vittal, K.P. Recent Developments in Control Schemes of BLDC Motors. In Proceedings of the IEEE International Conference on Industrial Technology (ICIT 2006), Mumbai, India, 15–17 December 2006; pp. 477–482.
8. Iizuka, K.; Uzuhashi, H.; Kano, M.; Endo, T.; Mohri, K. Microcomputer control for sensorless brushless motor. *IEEE Trans. Ind. Appl.* **1985**, *21*, 595–601. [[CrossRef](#)]
9. Serizawa, Y.; Iizuka, K.; Senou, M. Inverter controlled rotary compressors. *Hitachi Rev.* **1987**, *36*, 177–185.
10. Shen, J.X.; Liu, Y.B. Microcomputer Based Position-Sensorless Drive for Brushless DC Motor. In Proceedings of the International Power Electronics and Motion Control Conference, Beijing, China, 27–30 June 1994; pp. 402–407.
11. Zhu, Z.Q.; Ede, J.D.; Howe, D. Design criteria for brushless dc motors for high-speed sensorless operation. *Int. J. Appl. Electromagn. Mech.* **2001/2002**, *15*, 79–87.
12. Jahns, T.M.; Becerra, R.C.; Ehsani, M. Integrated current regulation for a brushless ECM drive. *IEEE Trans. Power Electron.* **1991**, *6*, 118–126. [[CrossRef](#)]

13. Moreira, J. Indirect sensing for rotor flux position of permanent magnet ac motors operating over a wide speed range. *IEEE Trans. Ind. Appl.* **1996**, *32*, 1394–1401. [[CrossRef](#)]
14. Kim, T.H.; Ehsani, M. An Error Analysis of the Sensorless Position Estimation for BLDC Motors. In Proceedings of the Conference Record Industry Applications Conference, Salt Lake City, UT, USA, 12–16 October 2003; pp. 611–617.
15. Niasar, A.H.; Vahedi, A.; Moghbelli, H. A novel position sensorless control of a four-switch, brushless dc motor drive without phase shifter. *IEEE Trans. Power Electron.* **2008**, *23*, 3079–3087. [[CrossRef](#)]
16. Shen, J.X.; Tseng, K.J. Analyses and compensation of rotor position detection error in sensorless PM brushless DC motor drives. *IEEE Trans. Energy Convers.* **2003**, *18*, 87–93. [[CrossRef](#)]
17. Urasaki, N.; Senjyu, T.; Uezato, K.; Funabashi, T. Adaptive dead-time compensation strategy for permanent magnet synchronous motor drive. *IEEE Trans. Energy Convers.* **2007**, *22*, 271–280. [[CrossRef](#)]
18. Kim, T.; Kim, C.; Lyou, J. A New Sensorless Drive Scheme for a BLDC Motor Based on the Terminal Voltage Difference. In Proceedings of the Conference of the IEEE Industrial Electronics Society, Melbourne, VIC, Australia, 7–11 November 2011; pp. 1710–1715.
19. Li, B.S.; Ma, R.X.; Fu, F.C.; Jin, X.H.; Chen, W. A New Sensorless Control Method for Brushless Permanent Magnet DC Motors. In Proceedings of the IEEE International Symposium on SLED/PRECEDE, München, Germany, 17–19 October 2013.
20. Bhogineni, S.; Rajagopal, K.R. Position Error in Sensorless Control of Brushless DC Motor Based on Average Line to Line Voltages. In Proceedings of the IEEE International Conference Power Electronics Drives Energy Systems, Bengaluru, India, 16–19 December 2012; pp. 1–6.
21. Lee, A.C.; Wang, S.; Fan, C.J. A current index approach to compensate commutation phase error for sensorless brushless dc motors with nonideal back EMF. *IEEE Trans. Power Electron.* **2016**, *31*, 4389–4399. [[CrossRef](#)]



© 2017 by the authors. Licensee MDPI, Basel, Switzerland. This article is an open access article distributed under the terms and conditions of the Creative Commons Attribution (CC BY) license (<http://creativecommons.org/licenses/by/4.0/>).